Annals of Nuclear Energy 83 (2015) 422–435

Contents lists available at ScienceDirect

Annals of Nuclear Energy

journal homepage: www.elsevier.com/locate/anucene

Experimental investigation and CFD analysis on cross flow in the core of PMR200

Jeong-Hun Lee [a], Su-Jong Yoon [b], Hyoung-Kyu Cho [a,*], Moosung Jae [c], Goon-Cherl Park [a]

[a] Department of Nuclear Engineering, Seoul National University, 1 Gwanak-ro, Gwanak-gu, Seoul 151-744, South Korea
[b] Idaho National Laboratory, 2525 Fremont Avenue, Idaho Falls, USA
[c] Department of Nuclear Engineering, Hanyang University, 222 Wangsimni-ro, Seongdong-gu, Seoul 133-791, South Korea

ARTICLE INFO

Article history:
Received 17 September 2014
Received in revised form 2 April 2015
Accepted 3 April 2015
Available online 16 April 2015

Keywords:
VHTR
PMR200
Bypass flow
Cross flow
Pressure loss coefficient
CFD

ABSTRACT

The Prismatic Modular Reactor (PMR) is one of the major Very High Temperature Reactor (VHTR) concepts, which consists of hexagonal prismatic fuel blocks and reflector blocks made of nuclear grade graphite. However, the shape of the graphite blocks could be easily changed by neutron damage during the reactor operation and the shape change can create gaps between the blocks inducing the bypass flow. In the VHTR core, two types of gaps, a vertical gap and a horizontal gap which are called bypass gap and cross gap, respectively, can be formed. The cross gap complicates the flow field in the reactor core by connecting the coolant channel to the bypass gap and it could lead to a loss of effective coolant flow in the fuel blocks. Thus, a cross flow experimental facility was constructed to investigate the cross flow phenomena in the core of the VHTR and a series of experiments were carried out under varying flow rates and gap sizes. The results of the experiments were compared with CFD (Computational Fluid Dynamics) analysis results in order to verify its prediction capability for the cross flow phenomena. Fairly good agreement was seen between experimental results and CFD predictions and the local characteristics of the cross flow was discussed in detail. Based on the calculation results, pressure loss coefficient across the cross gap was evaluated, which is necessary for the thermo-fluid analysis of the VHTR core using a lumped parameter code.

1. Introduction

The Very High Temperature Reactor (VHTR), one of the Generation-IV (Gen-IV) reactors, is uranium-fueled, graphite-moderated and helium-cooled reactor. It has several advantages of enhanced fuel integrity, proliferation resistance, relatively simple fuel cycle and modularity to supply electricity (Gauthier et al., 2006). Prismatic Modular Reactor (PMR) is one of the prospective VHTR type candidates and it was reported that the graphite block shape has advantages for neutron economy and high temperature structural integrity (Baxter et al., 2000). For these benefits, KAERI (Korea Atomic Energy Research Institute) in Korea has been developing a 200-MW (thermal) prismatic VHTR, PMR200, which adopted the prismatic fuel type as a promising candidate reactor for the Nuclear Hydrogen Development and Demonstration (NHDD) project (Jo et al., 2008).

The core of PMR200 consists of assemblies of hexagonal graphite fuel blocks and reflector blocks as shown in Fig. 1(a). The active core region includes 66 columns of fuel blocks and 6 fuel blocks are stacked vertically forming a single column. The fuel columns are arranged in an annulus with columns of hexagonal graphite reflector blocks in the central and outer regions. A fuel block contains 210 blind holes for fuel compacts and 108 through holes for coolant channels. Between the fuel blocks, there exist vertical and horizontal gaps for reloading of the fuel elements. The gaps can be enlarged and their shapes can be changed by thermal expansion and fast-neutron induced shrinkage (General Atomics, 1988). Thus, a certain portion of the helium coolant can flow through these gaps between fuel blocks; the flow that passes through the vertical gaps is called a bypass flow and one through the horizontal gaps is called a cross flow as depicted in Fig. 1(b). Since these gap flows can reduce the effective core flow rate during both of normal operation and abnormal conditions, prediction of them is important to evaluate the core cooling performance and safety of reactors.

The main interest of the present study is on the cross flow in the PMR200 core. The cross flow is often considered as a leakage flow through the horizontal gap between stacked fuel blocks. It complicates the flow distribution in the reactor core by connecting the

* Corresponding author. Tel.: +82 2 880 8339; fax: +82 2 889 2688.
E-mail address: chohk@snu.ac.kr (H.-K. Cho).

http://dx.doi.org/10.1016/j.anucene.2015.04.002
0306-4549/

Nomenclature

a	length of one edge of the hexagonal interface at the cross gap
CR	ratio of mass flow rate at the cross gap to outlet of the downstream block
Eu	Euler number
K	pressure loss coefficient
m_{cross}	mass flow rate at the cross gap
m_{main}	mass flow rate at the outlet of the downstream block
P	wetted perimeter
P_{wedge}	wetted perimeter for the wedge-shaped gap
$P_{parallel}$	wetted perimeter for the parallel gap
Re	Reynolds number
Re_{gap}	Reynolds number at the cross gap opening
v	velocity of air
ΔP	pressure difference
δ	gap width
μ	dynamic viscosity
ρ	density of air
ϕ	extrapolated solution by Richardson extrapolation method

coolant channel and the bypass gap as illustrated in Fig. 1(b). The cross flow can induce non-uniform core flow distribution and consequently, local superheating in fuel element zones with increased fission product release. On this aspect, the core cross flow has a negative impact on safety and efficiency of PMR200 and thus, it has to be investigated to evaluate the thermal margin of PMR200 more accurately (INEEL, 2003).

There are previous experimental works on the cross flow such as experiments conducted by Groehn (1982) in Germany and Kaburaki and Takizuka (1990) in Japan. In these experimental works, the pressure loss coefficients for the cross gap were obtained and based on the experimental data, correlations for the pressure loss coefficients were proposed. The pressure loss coefficient plays a crucial role in determining the flow rate at the cross gap in the thermo-fluid analysis using a lumped parameter code, which does not model the detail gap geometry between fuel blocks but model it using simplified pipe network approach with pressure loss terms. However, the correlations developed by the previous works are inapplicable to the PMR200 core analysis because the shapes of fuel blocks in those studies differ from those of PMR200 considerably. The number of coolant channels and the size of the channel in the fuel block are different between Groehn's study and current study. The fuel block in Groehn's experiment has 72 coolant holes of which diameter is 18 mm but that in PMR200 has 108 coolant holes with 13 mm (6 holes in the central region of the hexagon) and 16 mm (102 in the other region) diameters. In the case of Kaburaki's study, pin-in block type was applied, which has the fuel rods inserted into the coolant channels of the graphite block. Thus, it has annular cooling channels but PMR200 has circular ones. Due to these geometrical differences among previous works and the present work, the findings in the previous experiments cannot be directly applied to the PMR200 core analysis and the present experiment was motivated.

The objectives of this study are to provide experimental data for the cross flow rate in the PMR200 core and to evaluate the pressure loss coefficients of the cross flow. For this purpose, an experimental facility which has two stacked full-scale fuel blocks was constructed to represent the cross flow phenomena. Between the fuel blocks, an adjustable gap was installed and the cross flow rates were measured with various gap sizes in two different gap geometries: the wedge-shaped gap and parallel gap. After that, a commercial computational fluid dynamics code, ANSYS CFX 13 was validated to confirm its applicability to the cross flow phenomena by comparing the experimental data of the cross flow rates with the predicted ones. Finally, the pressure loss coefficients for the cross gap were evaluated from the validated CFD analysis results.

This paper presents the description of the experimental test facility and conditions, the experimental results, the calculation conditions of the CFD analyses and the CFD simulation results.

2. Cross flow experiment for the core of PMR200

2.1. Experimental facility and conditions

In order to understand the cross flow phenomena and quantify the cross flow, a cross flow experiment facility was designed and constructed, which consists of two stacked fuel blocks in full scale. The schematic view of experimental apparatus was illustrated in Fig. 2. In this experiment, the air at the ambient pressure and temperature was used as a working fluid instead of the high-temperature high-pressure helium. Hence, the scaling analysis is required to maintain the similarity between the proto and the experimental facility. In this study, in order to achieve dynamic similarity, Re number and Euler number in the coolant channel were preserved. The Euler number is a dimensionless number which expresses the ratio between a local pressure drop over a restriction and the kinetic energy per volume and is used to characterize losses in the flow. The definition of the Euler number is

$$Eu = \frac{\Delta P}{\rho v^2}, \tag{1}$$

where the ΔP is the pressure difference between inlet and outlet coolant channel of the fuel block, ρ is the density of the fluid, and v is the velocity of the fluid in the coolant channel. So as to preserve similarity, the conditions of the experiments were set to cover the normal operation condition of the PMR200 core. The main variables used for scaling analysis were summarized in Table 1.

The experimental facility consists of mainly air inlet pipes, test section, outlet pipes and a blower. The blower was installed at the lower part of the experimental facility and the suction part of the blower was connected to the outlet pipe of the test section. The air flows into the test section from the top of the inlet pipes which are long enough for the fully developed flow. After that, the air flows through the test section from the upstream block to the downstream one and discharges through outlet pipes and blower.

The two blocks have the same geometry with the PMR200 standard fuel block; its height and flat-to-flat width are 793 mm and 360 mm, respectively, and each one has 108 coolant holes. As shown in Fig. 2, the diameter of the coolant holes is 16 mm except for 6 holes in the center. The diameter of the 6 central holes is 12 mm. The cross gap was placed between two stacked fuel blocks. The neutron flux varies over the cross section of the core. It decreases with increasing distance from the center. Since the fuel block shrinks because of the neutron flux, it undergoes different axial shrinkage, which makes wedge-shaped gap. On the other hand, thermal deformation could lead to swelling of the fuel block causing parallel gap. In addition, a fuel block can be lifted by surrounding fuel blocks generating parallel cross gap. Hence, in the present experiments, two types of gap geometries, a wedge-shaped

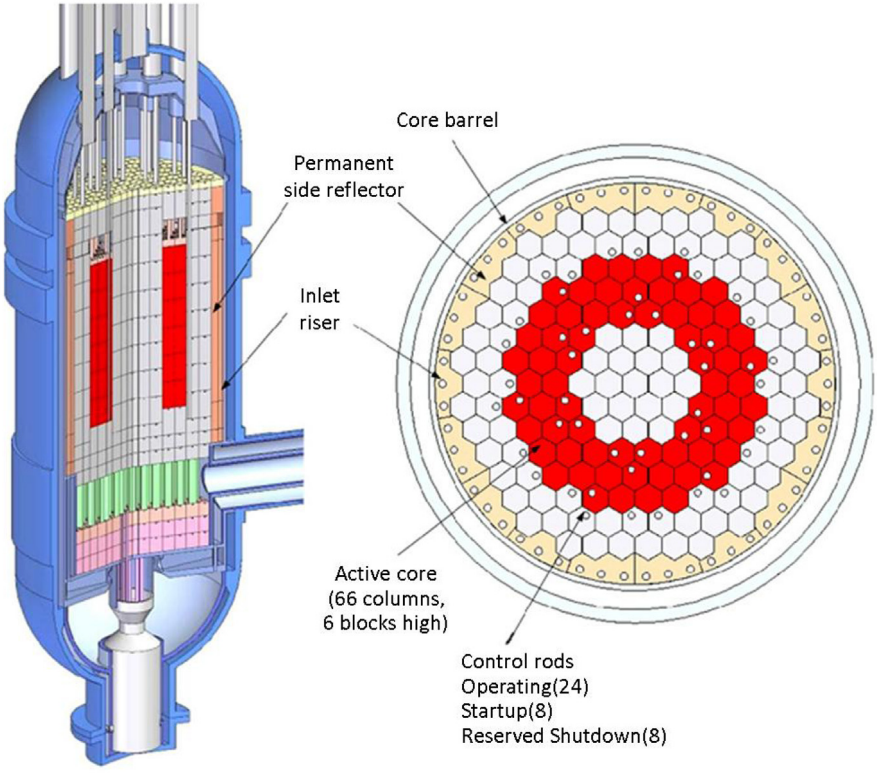

(a) Reactor vessel and top view of the reactor core

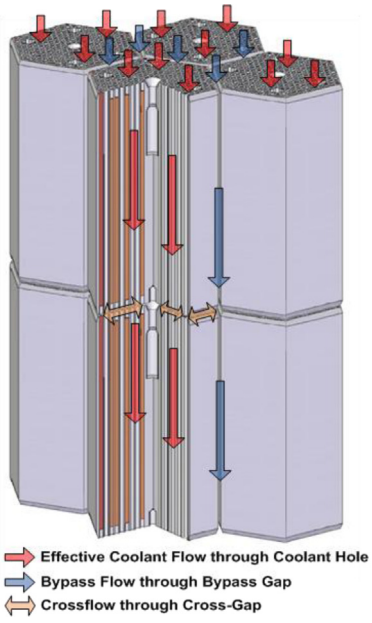

(b) Reactor core flows

Fig. 1. Reactor vessel and core of PMR200.

gap and a parallel gap, were applied by replacing the plate between the two fuel blocks as depicted in Fig. 3. The types of gaps which were tested in this study were described in Fig 4. The sizes of the gaps, δ, were set to be 0.5, 1, 2, 4, and 6 mm. The maximum size of the gap was selected to 6 mm according to the maximum gap size of the previous experimental studies (Groehn, 1982; Kaburaki and Takizuka, 1990) and the minimum size of the gap was selected to 0.5 mm considering the accuracy of the measurement.

For the experimental conditions, the outlet flow rates were set to be 0.1–1.35 kg/s which are evaluated to be ranged between 4000 and 54000 in Re numbers at a coolant channel. Since the Re number under normal operation condition is known to be approximately 23000, the test conditions cover the normal operation

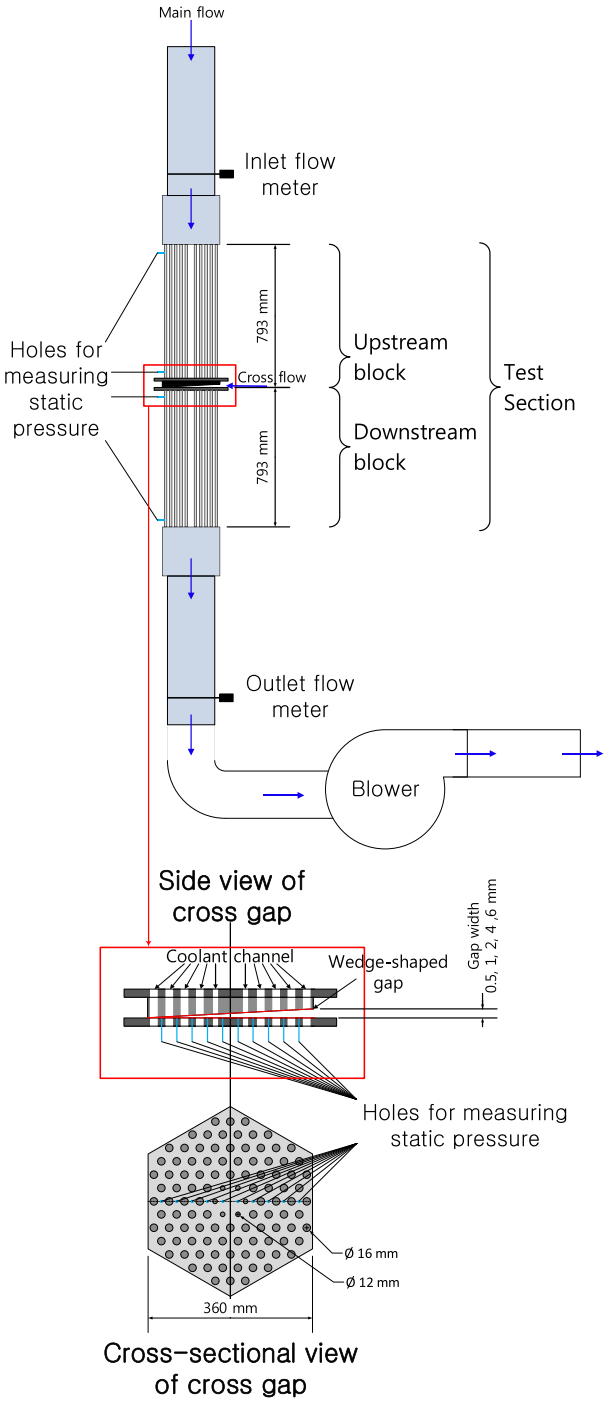

Fig. 2. Schematic view of experimental apparatus.

condition of the reference plant sufficiently. At the minimum flow rate and the maximum flow rate, the pressure differences between outside of the cross gap and 108 inlets of the downstream block coolant holes are around 10 Pa and 2500 Pa, respectively. The test matrix was summarized in Table 2 and a series of experiments were conducted with 355 test conditions varying shape and size of the gap and main flow rate.

The measurement variables and their instruments were listed in Table 3. The inlet flow rate of the upstream block, the outlet flow rate of the downstream block, the static pressures in the coolant channels and the pressure distribution in the cross gap were measured in this experimental facility. The cross flow rate was evaluated from the difference between measured inlet and outlet flow rates. Averaging Pitot Tubes were installed for measuring inlet flow rate and outlet flow rate. Pressure transmitters were used to measure static pressures in the coolant channels and in the cross gap. The uncertainties of the measured variables were summarized in Table 4.

2.2. Experimental results

Figs. 5 and 6 present the experimental results of the cross flow rate for whole cases. The absolute value of the cross flow rate increases with the main flow rate as seen in Fig. 5(a) and (b). In the cases of parallel gap, the cross flow rate is obviously larger than that in the wedge-shaped gap cases because the parallel cross gap has twice larger area than the wedge-shaped gap. In order to find out the characteristics of cross flow, the ratio of the cross flow rate to the main flow rate was plotted as presented in Fig. 5(c) and (d). The ratio of the cross flow rate, *CR*, can be expressed as

$$CR = \frac{m_{cross}}{m_{main}}, \tag{2}$$

where m_{cross} is the mass flow rate of the cross flow and the m_{main} is the main flow rate which means the outlet mass flow rate of the downstream block. Since the cross flow rate increases linearly with the main flow rate as shown in Fig. 5, the ratio of the cross flow rate has almost constant value as plotted in Fig. 5(c) and (d). It means the ratio of the cross flow is more affected by the size of the gap than by the main flow rate and, therefore, the shape and size of the gap are the important factors of the cross flow. Even though the ratio of the cross flow rate is nearly constant for each gap size, it decreases slightly with increasing main flow rate when the gap size is 6.0 mm, while it increases when the gap size is 0.5 mm. In order to figure out the reason of this opposite trend depending on the gap size, the experimental results were analyzed with the gap Re number and the cross flow ratio to the dimensionless number was plotted as presented in Fig. 6. The gap Re number is defined as

$$\mathrm{Re}_{gap} = 4\frac{m_{cross}}{\mu P}, \tag{3}$$

Table 1
Main variables for scaling analysis.

	PMR200 normal operation	Experiment	Degree of similitude
Working fluid	Helium at 7 MPa	Air at ambient pressure	–
Density (kg/m^3)	3.868	1.185	0.31
Viscosity (Pa·s)	4.111×10^{-5}	1.841×10^{-5}	0.45
Mass flow rate (kg/s)	1.192	0.565	0.47
Velocity (m/s)	15.26	22.3	1.46
Pressure drop in one fuel block (Pa)	578.6	378.7	0.65
Reynolds number	22793	22795	1
Friction factor	0.02572	0.02572	1
Euler number	0.6423	0.6423	1

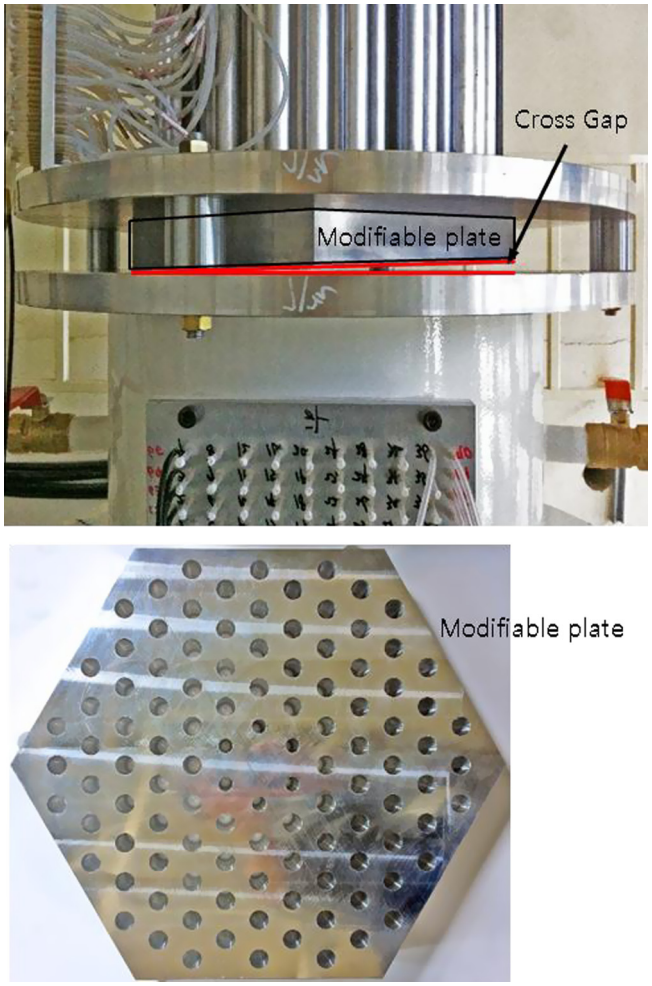

Fig. 3. Experimental apparatus and cross gap.

where μ is the dynamic viscosity of the air and P is the wetted perimeter which is expressed as

$$P_{wedge} = 10a,$$
$$P_{parallel} = 12a, \quad (4)$$

where a is the length of one edge of the hexagonal interface at the cross gap. In the cases of wedge-shaped gap, the air flows into 5 faces of the cross gap opening. On the other hand, in the parallel gap cases, the air flows into 6 faces of the cross gap opening as shown in Fig. 4 and this caused the difference in the wetted perimeter expression.

Similar to Fig. 5(c) and (d), the cross flow ratio is nearly constant along the gap Re number. However, the slope of the graph exhibits different trend depending on the size of the gap when it is magnified. In the case of 6 mm wedge-shaped gap, the ratio of the cross flow decreases as the gap Re number increases as shown in Fig. 7. In this case, the range of the gap Re number is approximately 2000–21000 at 0.1–1.35 kg/s of the main flow rate as tabulated in Table 5, which means that the flow regime of this case is dominantly turbulent. In the case of 1.0 mm wedge-shaped gap, the ratio of the cross flow rate is almost constant (see Fig. 8). The gap Re numbers are approximately 500, 3400, and 4600 at 0.1 kg/s, 0.8 kg/s, and 1.35 kg/s of the main flow rates, respectively (Table 5). In these experimental conditions, the flow regime changes from laminar to turbulent. Fig. 9 shows the ratio of the cross flow rate of 0.5 mm wedge-shaped gap. In this case, the ratio of the cross flow increases with the gap Re number. The gap Re number in this case ranges from 350 to 2300 at main flow rate of 0.1–1.35 kg/s, which implies the flow regime in this case is dominantly laminar flow. In the cases of parallel gap, a consistent tendency with the wedged gap cases was observed as indicated in Figs. 10–12. The gap Re numbers for each case are also tabulated in Table 5. From these results of the experiments, it was deduced that the tendency of the cross flow ratio to the gap Re number is affected by the flow regime. The cross flow ratio increases with the gap Re number if the gap Re number is smaller than 1000 and then it maintains nearly constant value, after that, it decreases significantly when the gap Re number is over 5000.

3. CFD analysis

From the experiments, the mass flow rate of the cross flow and the ratio of the cross flow were obtained. In order to obtain the pressure loss coefficient at the cross gap, the averaged differential pressure between outside of the cross gap and 108 inlets of the downstream block coolant holes and the averaged velocity of the cross flow at cross gap openings are necessary. The latter was measured in the experiment but the former was unable to be measured due to difficulty in installation of the pressure taps for all coolant holes and due to inaccurate pressure measurement influenced by vena contracta. Therefore, in this study, the prediction capability of the CFD for this experiment was validated at first and then, the form loss coefficient of the cross flow was obtained from the CFD analysis results. In this section, the calculation conditions for the CFD analysis, validation results with the experimental data, and the form loss coefficient obtained from the CFD analysis were presented.

3.1. Numerical models and boundary conditions

In order to apply the CFD code, the prediction capability of CFX 13 was validated by comparing the calculation results from the experimental data. This section introduces the computational domain, boundary conditions, applied mesh, and physical models of the CFD analysis and the calculation results will be presented in the next section in conjunction with the experimental data.

Fig. 13 shows computational domain and mesh structure for the case of wedge-shaped gap with 6 mm width. In the present simulation, GAMBIT 2.2.30 was used for generating geometry and mesh grid. Approximately 9 million hexahedra mesh were used for the present simulation. Wall y^+ value was approximately 20. The working fluid used was air at ambient temperature and pressure. Since the pressure drop through two fuel blocks is under 5000 Pa at maximum flow rate condition, the properties of fluid were assumed to be constant. The Shear Stress Transport (SST) model of Menter (1994) with an automatic wall treatment based on the Reynolds Averaged Navier–Stokes (RANS) equation was adopted for turbulence modeling since the SST-k-ω model is able to produce good results for the flow with a separation. In addition, better results could be obtained by applying the transitional Gamma-Theta model (Langtry and Menter, 2005). The turbulence numeric and the advection fluxes were evaluated using a high resolution scheme that is second-order accurate and bounded in the current analyses. Residual for convergence criteria of iteration was set under 10^{-5}. The calculation conditions were set according to experimental conditions. The computational domain consists of the opening boundary condition, outlet boundary condition and wall boundary condition. The opening boundary condition was imposed on the entrance of the upstream block and the cross gap between blocks. In the boundary details, the Mass and

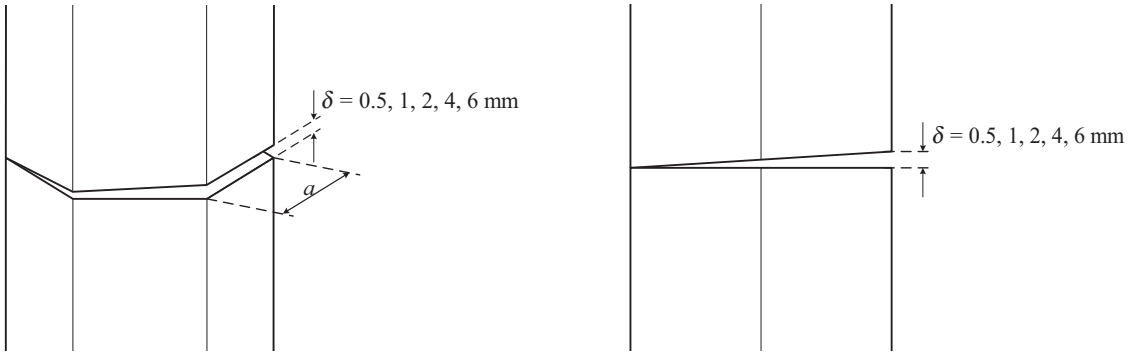

(a) Wedge-shaped gap

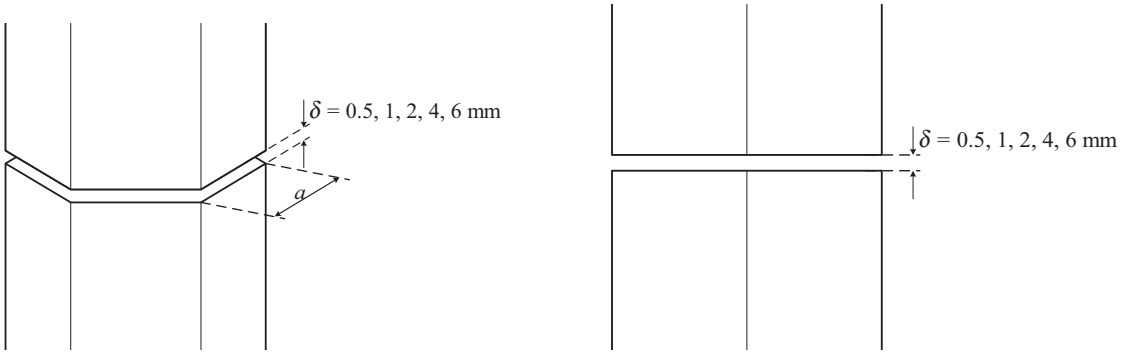

(b) Parallel gap

Fig. 4. Types of tested cross gaps.

Table 2
Test matrix.

Gap Shape	Gap width (mm)	Flow rate (kg/s)	Number of test cases	Temperature (°C)
Wedge	0.5	0.1–1.35	35	19
	1.0	0.1–1.35	35	18
	2.0	0.1–1.35	43	17
	4.0	0.1–1.35	35	16
	6.0	0.1–1.35	32	18
	Total		180	
Parallel	0.5	0.1–1.35	35	20
	1.0	0.1–1.35	35	21
	2.0	0.1–1.35	35	22
	4.0	0.1–1.35	35	23
	6.0	0.1–1.35	35	22
	Total		175	

Table 3
Measuring instruments.

Variable	Measuring instrument	Error
Flow rates	FCO68/Furness controls	0.1% of reading
Pressure transmitters for flow rate	Rosemount 3051/Rosemount	0.04% of span
Static pressures	VPRN-A2-(5–10) kPa-4C/Valcom	0.1% of reading

Momentum was set to be Opening Pres. and Dirn with a Relative Pressure of 0 Pa. The outlet of the downstream block was defined as the mass flow rate boundary condition. No slip wall and smooth wall were adopted as wall boundary conditions. Widths of the cross gaps were selected to be 0.5, 1, 2, 4, and 6 and outlet flow rates were varied from 0.1 to 1.35 kg/s as in the experiment.

Table 4
Uncertainties of the measured variables.

Variable	Uncertainty	
	Minimum flow rate condition (m_{main} = 0.1 kg)	Maximum flow rate condition (m_{main} = 1.35 kg)
ΔP	2.01 Pa (20.1%)	43.2 Pa (2.51%)
P	0.16%	0.16%
T	0.75%	0.75%
m_{main}	0.01 kg/s (10%)	0.023 kg/s (1.67%)
m_{cross}	0.014 kg/s (14% of m_{main})	0.032 kg/s (2.4% of m_{main})
CR (Cross flow Ratio)	17.5%	2.90%

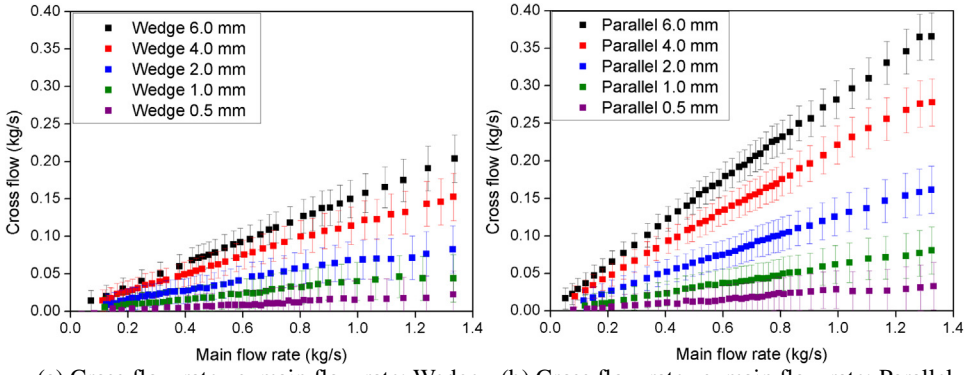

(a) Cross flow rate vs. main flow rate: Wedge (b) Cross flow rate vs. main flow rate: Parallel

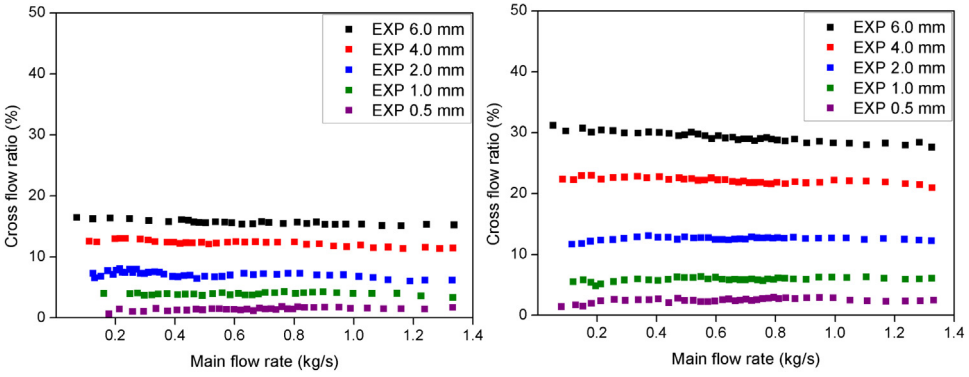

(c) Cross flow ratio vs. main flow rate: Wedge (d) Cross flow ratio vs. main flow rate: Parallel

Fig. 5. The cross flow rate and the cross flow ratio to the main flow rate.

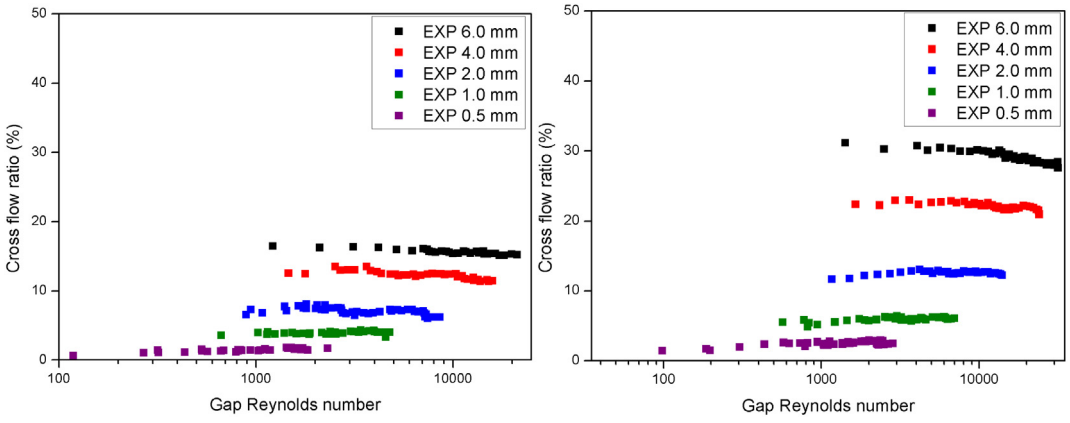

(a) Wedge-shaped gap (b) Parallel gap

Fig. 6. The ratio of the cross flow rate to the gap Re number.

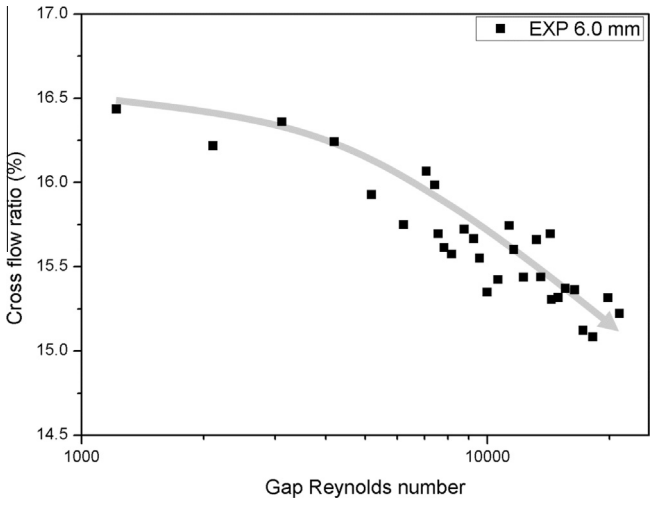

Fig. 7. The ratio of the cross flow rate: 6 mm wedge-shaped gap.

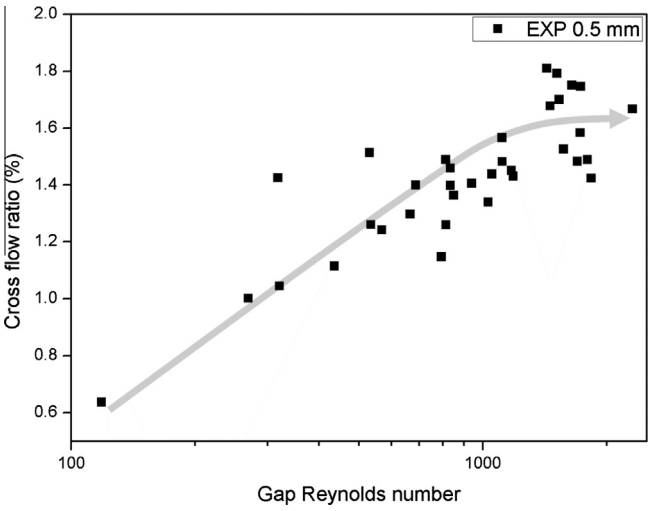

Fig. 9. The ratio of the cross flow rate: 0.5 mm wedge-shaped gap.

Table 5
Gap Reynolds number in experiments.

Shape	Gap width (mm)	Main flow rate (kg/s)	Re
Wedge	0.5	0.1	350
		1.35	2300
	1.0	0.1	500
		0.8	3400
		1.35	4600
	6.0	0.1	2000
		1.35	21000
Parallel	0.5	0.1	120
		1.35	3000
	1.0	0.1	450
		0.55	3000
		1.35	7100
	6.0	0.1	2600
		1.35	32000

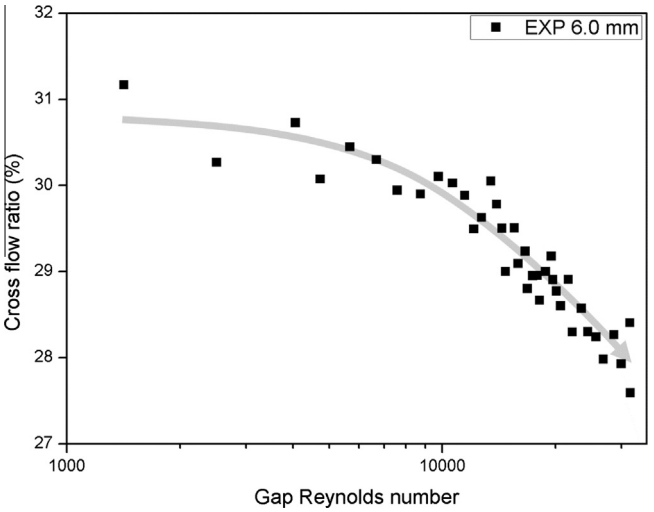

Fig. 10. The ratio of the cross flow rate: 6 mm parallel gap.

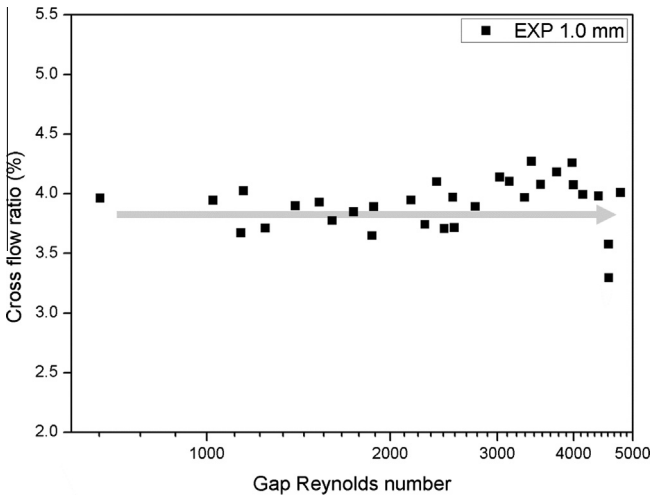

Fig. 8. The ratio of the cross flow rate: 1 mm wedge-shaped gap.

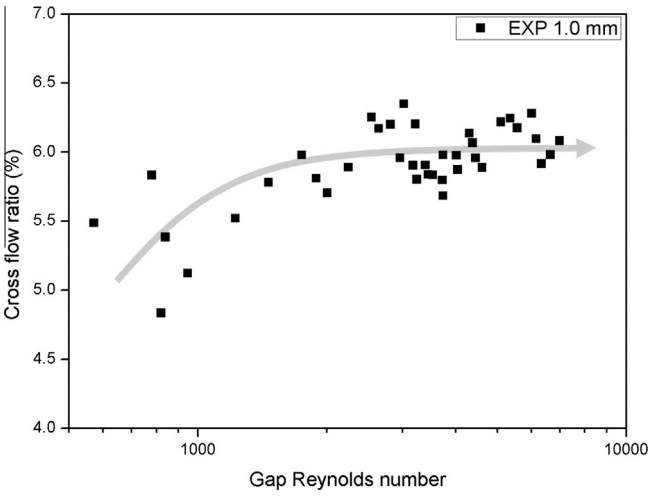

Fig. 11. The ratio of the cross flow rate: 1 mm parallel gap.

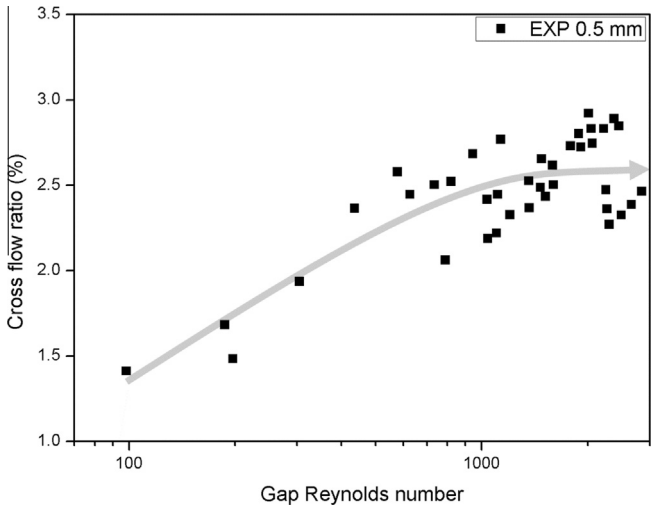

Fig. 12. The ratio of the cross flow rate: 0.5 mm parallel gap.

3.2. Grid convergence study

A grid convergence study was conducted using current grid (8.76 million cells) and coarser grid cases (3.98 million cells, 1.77 million cells and 0.81 million cells) with 1 kg/s outlet flow rate and 6 mm wedge-shaped gap. The meshes used in this grid convergence study are presented in Fig. 14. The mass flow rates at the cross gap and pressure drops from the inlet to the outlet were compared between the current and coarse mesh cases as plotted in Fig. 15. The extrapolate solution, ϕ, was obtained by using Richardson Extrapolation method (Richardson, 1910; Richardson and Gaunt, 1927). The differences in the mass flow rates at the cross gap and pressure drops at the outlet were summarized in Table 6. Since the estimated errors of the Mesh 4 case are under 1%, it was selected for this analysis and the results indicate that the current grid is sufficiently fine for simulating the cross flow phenomena in the two-stacked fuel block.

3.3. Comparison results between CFD calculation and experiment

In order to verify the prediction capability of the CFD code, the calculation results were compared with the experimental results in Figs. 16–18. In Figs. 16 and 17, the analysis results for the largest and smallest gaps are presented and the comparison results of whole cases are plotted in Fig. 18. As seen in Figs. 16 and 17, the results of the CFD calculation showed fairly good agreement with the experimental data. Especially, the increasing trend of the cross flow ratio with the small gap size and the reverse trend with the large gap size were well captured by the simulation. This means that for the fully laminar or turbulent regions, the present CFD analysis reproduced the cross flow phenomena accurately. However, slight discrepancies were observed with the wedged gap when its size is in the range of 1–2 mm. In general, the CFD calculation under-predicted the experimental data slightly when the main flow rate is low and accordingly, the Reynold number is low. Nevertheless, the disagreement of the results between the experiment and the CFD calculation is within 2% in the absolute value of the cross flow ratio. Fig. 19 presents the comparison between the experimental data and the CFD calculation results for whole cases. Considering the uncertainty of the experimental data is 2.4% at the maximum flow rate condition, the discrepancies can be considered insignificant.

Local flow behaviors in the cross gap were investigated from the CFD analysis results focusing on the laminar to turbulent transition in the gap. Fig. 20 shows the velocity streamlines in the 2 mm cross gap. As described in Fig. 20, the cross flow penetrates more deeply as the main flow rate increases. In the case of flow rate 0.1 kg/s, the cross flow is very week and the flow converges to the coolant holes near the center. As the main flow rate increases, the cross flow converges farther from opening of the cross gap. In Fig. 20, the

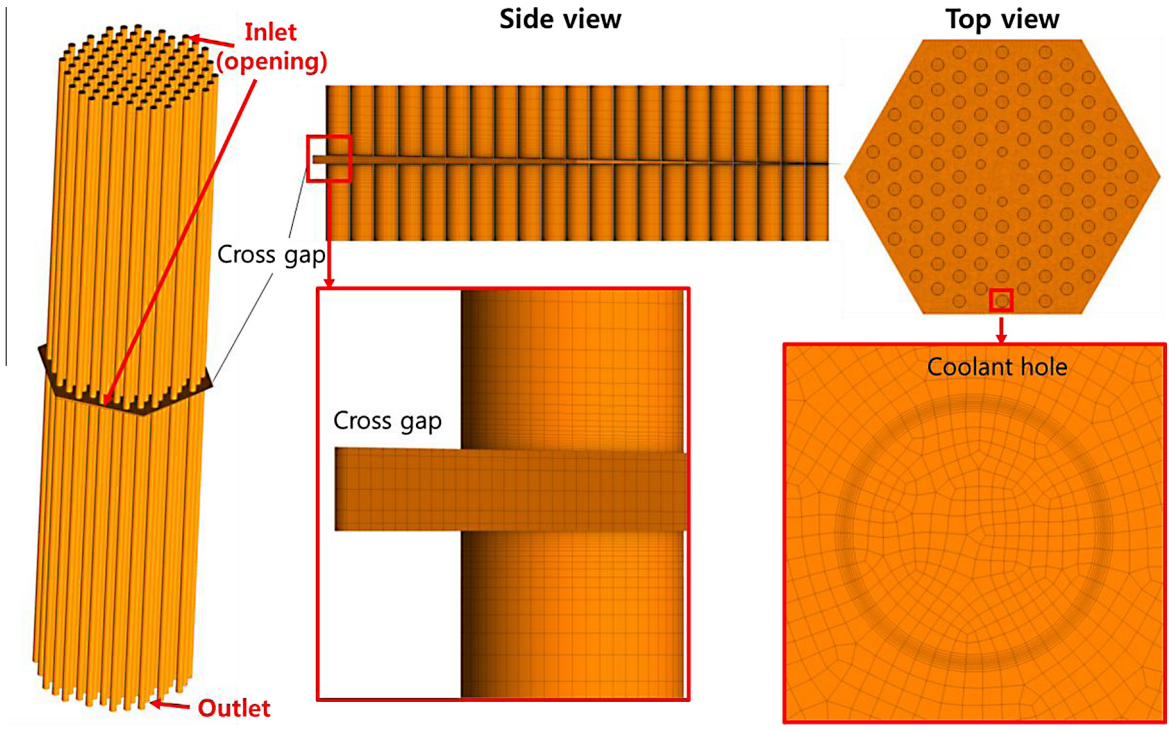

Fig. 13. Computational domain and mesh structure.

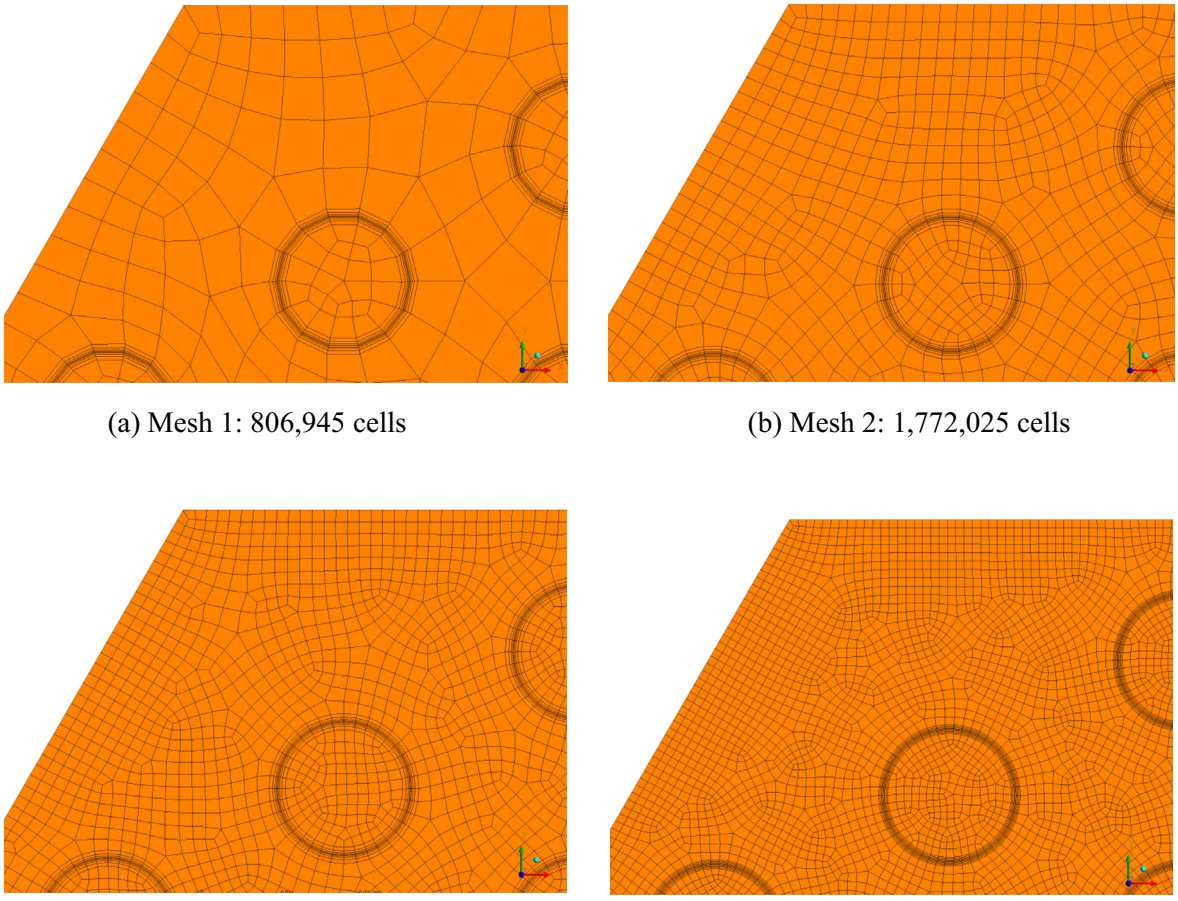

(a) Mesh 1: 806,945 cells

(b) Mesh 2: 1,772,025 cells

(c) Mesh 3: 3,983,165 cells

(d) Mesh 4 (base case): 8,761,490 cells

Fig. 14. Finite element meshes used in grid convergence study.

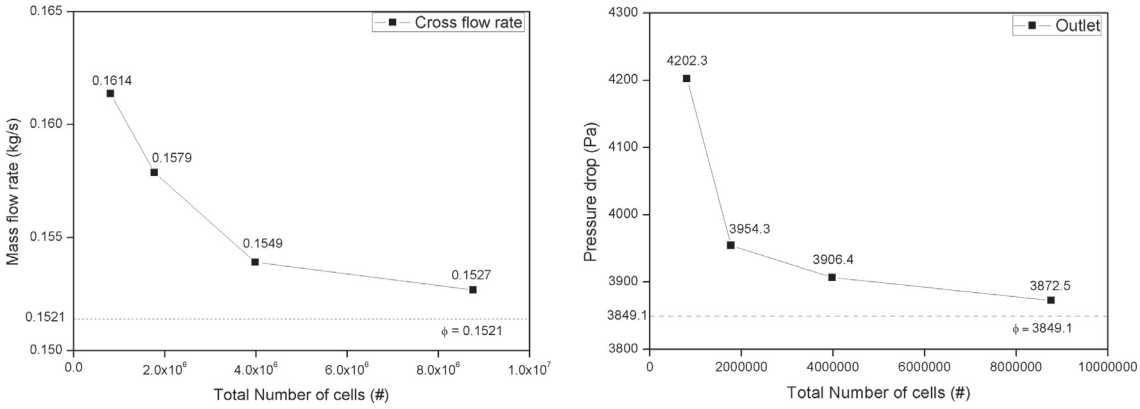

(a) Mass flow rate at the cross gap

(b) Pressure drop from inlet to the outlet

Fig. 15. Grid convergence test.

gap Re numbers are 570, 3000, and 7800 with the main flow rates 0.1, 0.5, and 1.35 kg/s, respectively. It implies that there exists the flow regime change from laminar to turbulent.

Fig. 21 shows the streamline profile of the CFD analysis with 0.5 mm gap and 0.5 kg/s main flow rate. At this flow condition, the gap Re number is about 570. As expected, the streamlines show very similar profile to Fig. 20(a) which has comparable gap Re number. In the same manner, the velocity streamlines in Fig. 22 with 6 mm gap and Re number of 8100 shows analogous profile with Fig. 20(c). From this analysis, it was found that the velocity profile in the cross gap strongly depends on the flow regime and the gap Re number rather than the Re number of the main flow.

3.4. Pressure loss coefficient

The pressure loss coefficient in the cross gap plays a crucial role when estimating the cross flow rate using a lumped parameter code, which is used frequently for the safety and performance

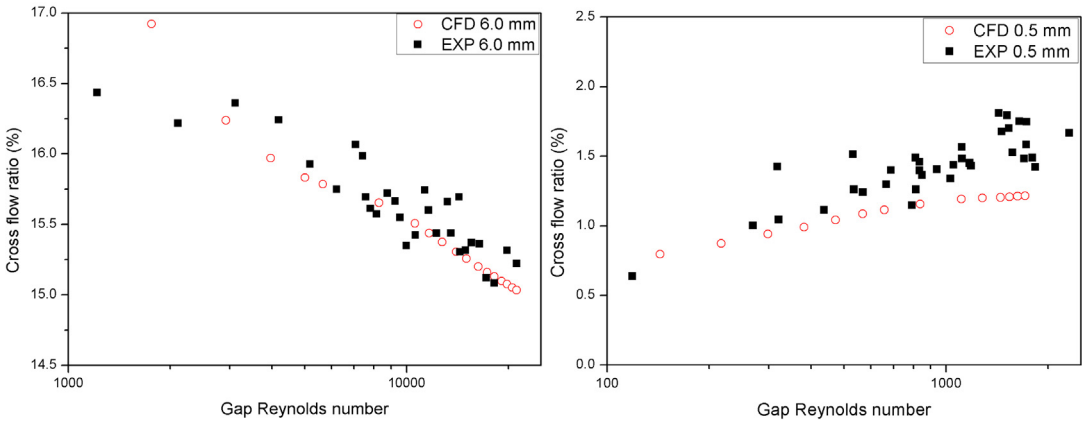

(a) Gap size 6 mm case (b) Gap size 0.5 mm case

Fig. 16. Comparison results for the wedge-shaped gap cases.

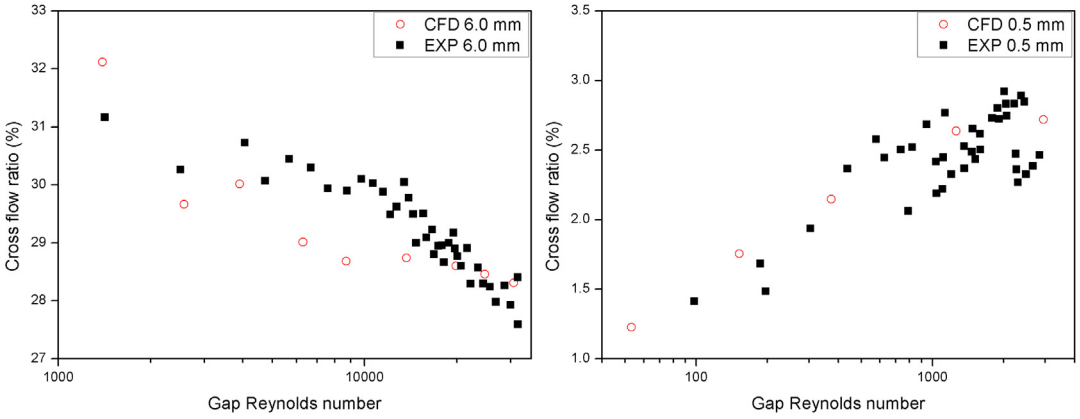

(a) Gap size 6 mm case (b) Gap size 0.5 mm case

Fig. 17. Comparison results for the parallel gap cases.

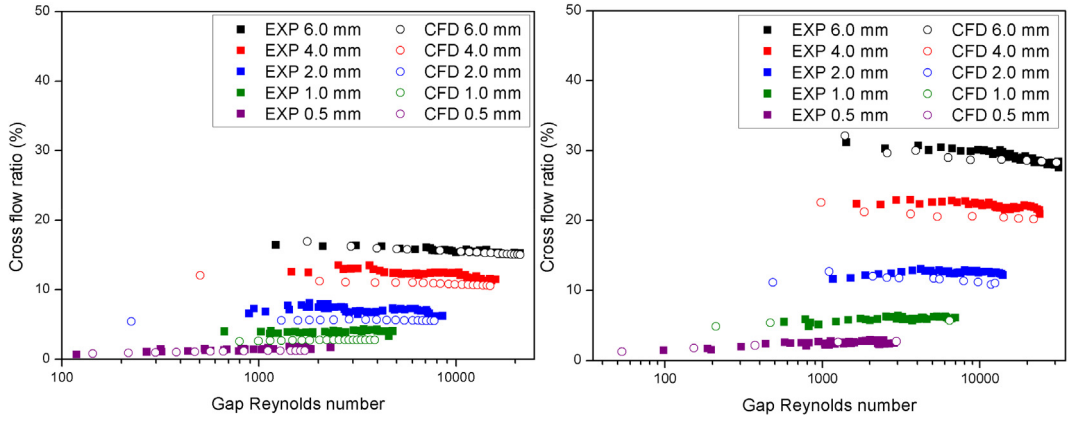

(a) Wedge-shaped gap (b) Parallel gap

Fig. 18. Comparison results for whole cases.

analysis of a prismatic core of VHTR. Such a code determines the cross flow rate from the pressure difference between two fuel blocks and the pressure loss across the cross gap. In order to provide the loss coefficients for the lumped parameter codes, the variables from CFD analysis results were analyzed. The loss coefficient, K, is defined as

$$K = \frac{\Delta P}{\frac{1}{2}\rho v^2}, \tag{5}$$

Table 6
Grid convergence test results.

Case	Total number of elements	Flow rate at the cross gap [kg/s]	Error of cross flow rate [%]	Pressure drop at the outlet [Pa]	Error of pressure drop [%]
Mesh 1	806,945	0.161357	6.09	4202.3	9.18
Mesh 2	1,772,025	0.157865	3.79	3954.3	2.73
Mesh 3	3,983,165	0.153901	1.18	3906.5	1.45
Mesh 4	8,761,490	0.152674	0.38	3872.5	0.61
Richardson solution, ϕ	–	0.1521	–	3849.1	–

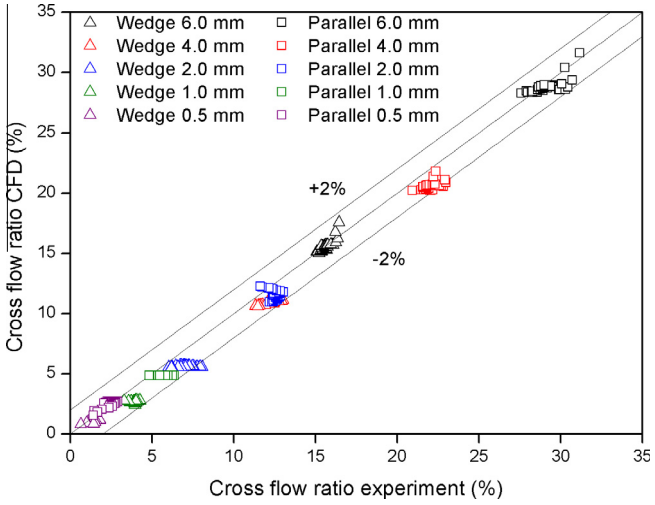

Fig. 19. Comparison of the CFD prediction and experiments for whole cases.

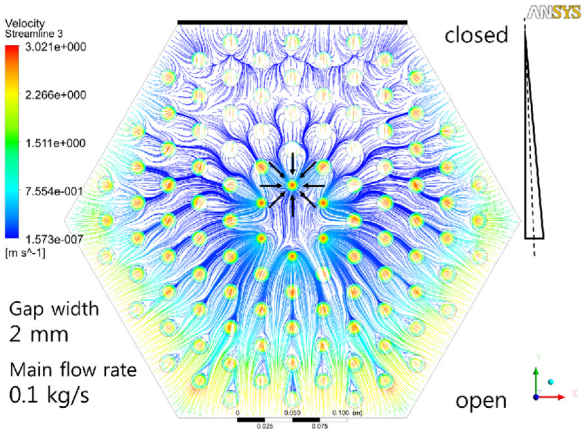

(a) Gap width 2 mm, main flow rate 0.1 kg/s

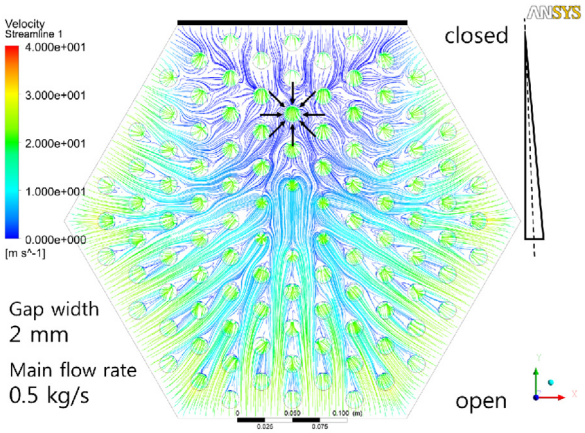

(b) Gap width 2 mm, main flow rate 0.5 kg/s

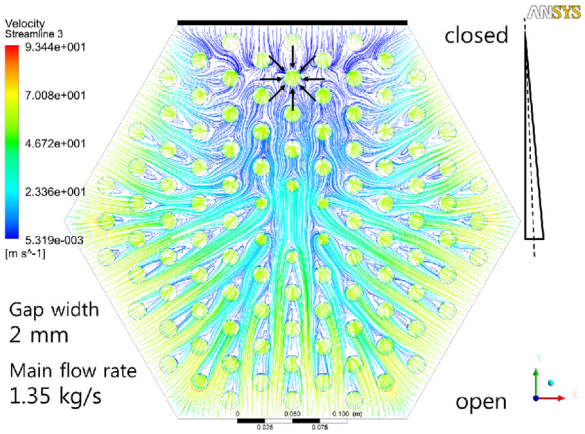

(c) Gap width 2 mm, main flow rate 1.35 kg/s

Fig. 20. Velocity streamline of the wedge-shaped gap of 2 mm width.

where ΔP is the pressure drop between outside of the cross gap and the inlet of the downstream fuel block at the cross gap and v is the average velocity of the cross flow at the cross gap opening. In order to obtain the loss coefficients for the cross gap, the pressures at entire coolant channels need to be averaged and the averaged value was obtained from the CFD calculation results. For consistency, velocity of the cross flow at the cross gap opening was also calculated with the CFD.

The loss coefficients with the wedge-shaped gap and parallel gap are plotted in Fig. 23 along the gap Re number. The pressure loss coefficient of the cross flow decreases as the gap Re number increases until 2000 and above it, the loss coefficient becomes constant. This is correspondent with the trend of the friction factor in rough pipes. According to the friction factor of the Darcy–Weisbach equation (Moody, 1944), it is inversely proportional to the Re number in laminar flow but it becomes almost constant in turbulent flow, depending only on the pipe roughness. A similar trend was obtained in the present experiment. The tendency of the variation of the cross flow ratio with the gap Re number can be interpreted by this characteristic of the loss coefficient. Since the loss coefficient decreases with the gap Re number if it is lower than 2000, the ratio of the cross flow increases as seen in the graphs of the gap size 0.5 mm cases (see Figs. 9, 12, 16(b) and 17 (b)).

From this analysis, it can be concluded that the cross flow is governed by the gap Re number and it implies the cross flow shows different behavior according to flow regime. This analysis results will be used in order to develop a correlation for the pressure loss coefficient, which is required for the prediction of the cross flow rate using a lumped parameter code.

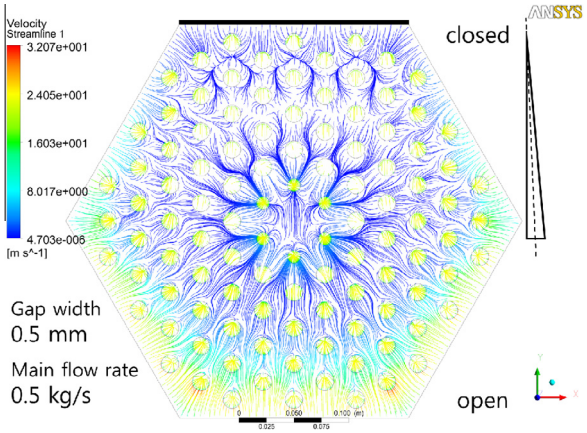

Fig. 21. Velocity streamline of 0.5 mm wedge-shaped gap and 0.5 kg/s main flow rate.

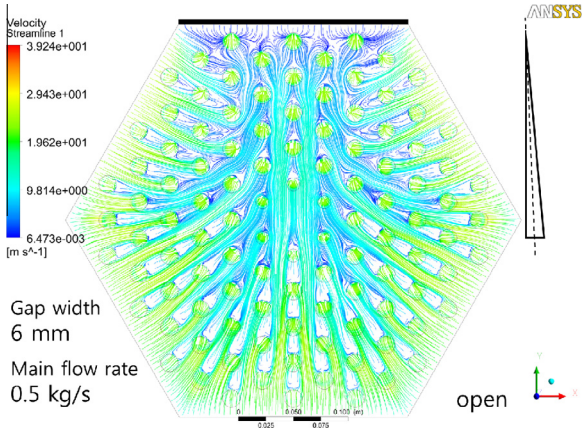

Fig. 22. Velocity streamline of 6 mm wedge-shaped gap and 0.5 kg/s main flow rate.

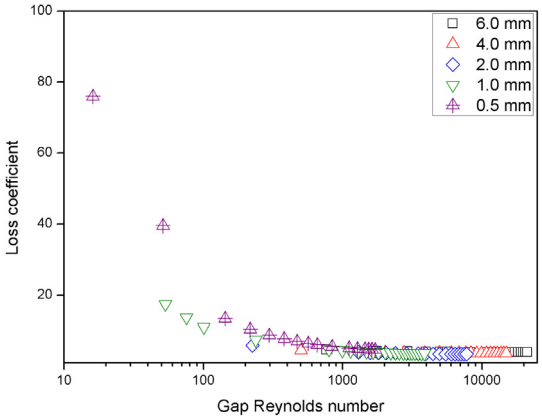

(a) Wedge-shaped gap

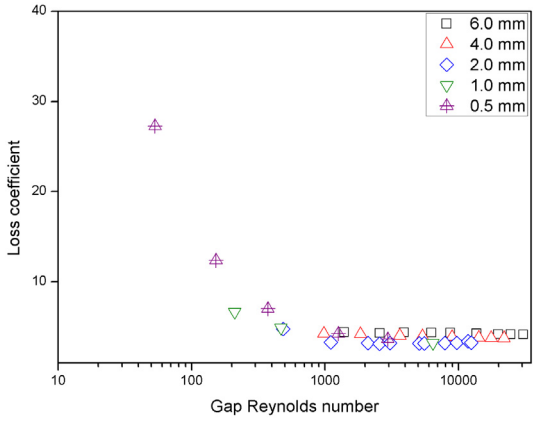

(b) Parallel gap

Fig. 23. Pressure loss coefficient at the cross gap.

4. Conclusions

In the present paper, in order to understand the cross flow phenomena in the core of PMR200, a series of experiments were conducted. Two different types of cross gaps, wedge-shaped gap and parallel gap, were used for the experiments and the cross flow rates were measured varying gap sizes and flow rates. In addition, CFD analysis was performed to validate its prediction capability, to investigate local phenomena and to evaluate the pressure loss coefficient across the cross gap. Conclusions can be summarized as follows:

- The results of the CFD analysis and experimental data are in good agreement even though CFD slightly underestimates in laminar-turbulent transitional region.
- The ratio of the cross flow is significantly affected by the cross gap size rather than the main flow rate.
- The cross flow ratio increases with the main flow rate if the gap Re number is smaller than 2000, but decreases if it is sufficiently large to establish a turbulent flow. The flow pattern inside the cross gap is also governed by the gap Re number.
- The pressure loss coefficient for the cross gap between the fuel blocks of PMR200 was obtained. The pressure loss coefficient of the cross flow decreases as the Re number increases until 2000 and becomes constant in high Re region.

Further study will be followed to develop the correlation of the cross flow loss coefficient, and then the correlation will be used to thermal–hydraulic analysis codes for the prismatic VHTR that incorporate lumped parameter model for a graphite block.

Acknowledgement

This work was supported by a Basic Atomic Energy Research Institute (BAERI) Grant funded by the Korean government Ministry of Education and Science Technology (MEST) (NRF-2010-0018759).

References

Baxter, A., Rodriguez, C., Richards, M., Kuzminski, J., 2000. helium-cooled reactor technologies for accelerator transmutation of nuclear waste. In: Proceedings of 6th Information Exchange Meeting on Actinide and Fission Product Partitioning and Transmutation, Madrid, Spain, December 11–13.

Gauthier, J.C., Brinkmann, G., Copsey, B., Lecomte, M., 2006. ANTARES: The HTR/VHTR project at Framatome ANP. Nucl. Eng. Des. 236, 526–533.

General Atomics, 1988. Graphite Design Handbook, DOE-HTGR-88111, Rev. 0.

Groehn, H.G., 1982. Estimate of cross flow in high temperature gas-cooled reactor fuel blocks. Heat Transfer Fluid Flow Nucl. Technol. 5, 392–400.

Idaho National Engineering and Environmental Laboratory, 2003. NGNP Preliminary Point Design – Results of the Initial Neutronics and Thermal-Hydraulic Assessment, INEEL/EXT-03-00870.

Jo, C.K., Lim, H.S., Noh, J.M., 2008. Preconceptual designs of the 200 MWth prism and pebble-bed type VHTR cores. In: Proceedings of International Conference on the Physics of Reactors. Interlaken, Switzerland, September 14–19.

Kaburaki, H., Takizuka, T., 1990. Crossflow characteristics of HTGR fuel blocks. Nucl. Eng. Des. 120, 425–434.

Langtry, R.B., Menter, F.R., 2005. Transition Modeling for General CFD Applications in Aeronautics. AIAA Journal, In: Proceedings of 43rd AIAA Aerospace Sciences Meeting, Reno, NV, USA, January 10–13.
Menter, F.R., 1994. Two-equation Eddy-viscosity turbulence models for engineering applications. AIAA J. 32, 1598–1605.
Moody, L.F., 1944. Friction factors for pipe flow. Trans. ASME 66, 671–684.
Richardson, L.F., 1910. The approximate arithmetical solution by finite differences of physical problems involving differential equations, with an application to the stresses in a masonry dam. Philos. Trans. R. Soc. London, Ser. A 210, 307–357.
Richardson, L.F., Gaunt, J.A., 1927. The deferred approach to the limit. Philos. Trans. R. Soc. London, Ser. A 226, 299–361.